ECS Transactions, 58 (14) 79-88 (2014)
10.1149/05814.0079ecst ©The Electrochemical Society

Structural Analysis and Electrochemical Studies of Carbon Coated $Li_4Ti_5O_{12}$ Particles Used as Anode for Lithium Ion Battery

Xiangcheng Sun[a*], M. Hegde[b], Jian Wang[c], Yuefei Zhang[d] , Jinyun Liao[a], P. V. Radovanovic[b] and Bo Cui[a]

[a]Department of Electrical and Computer Engineering, University of Waterloo, Canada
[b]Department of Chemistry, University of Waterloo, Canada
[c]Canadian Light Source Inc, Saskatoon, Canada
[d]Institute of Microstructure and Property of Advanced Materials, Beijing University of Technology, Beijing, China
*Email: sunxc824@gmail.com

Carbon coated $Li_4Ti_5O_{12}$ (C-LTO) particles have been synthesized by hydrothermal method and high-temperature calcination process. Nanostructure and carbon-coating has been characterized in detail by X-ray diffraction (XRD), high resolution TEM (HR-TEM), selected electron diffraction (SAED), and scanning transmission X-ray microscopy (STXM) combined with X-ray absorption near edge structure (XANES) spectroscopy. The prepared particles are comprised of highly crystalline spinel-type $Li_4Ti_5O_{12}$ with the size range of 20-70 nm. HR-TEM imaging and STXM-XANES spectromicrocopy confirmed the amorphous carbon layer uniformly covered on the surface of single LTO particles with optimized content and coating thickness (~5 nm). The electrochemical performance of C-LTO particles as an anode in lithium-ion batteries is evaluated, demonstrating both improved rate capability and cycling performance, which was attributed to the enhanced electron transport/high electrical conductivity and fast lithium-ion insertion/extraction, as a result of uniform and optimized amorphous carbon coating on the C-LTO particles.

Introduction

The spinel-type $Li_4Ti_5O_{12}$ (LTO) has attracted great interest as anode material of rechargeable lithium-ion batteries (LIBs) because of its unique characteristics: (1) zero strain during charging and discharging, (2) excellent cycle reversibility, (3) fast Li^+ insertion and de-insertion and (4) a relatively high lithiation voltage plateau at 1.55 V versus Li/Li^+, which can sufficiently avoid the formation of the insulating solid-electrolyte interphase (SEI), therefore improving the safety of LIBs [1-4]. All of these merits make LTO more competitive as a safe anode material for long life energy-storage LIBs. However, the high-rate performance of bulk LTO is hindered by its inherent low electrical conductivity (ca. 10^{-13} S cm^{-1}) and moderate Li^+ diffusion coefficient (10^{-8} cm^2 s^{-1}) [5], which cause the serious polarization of the electrode at high current densities.

The most commonly used strategies to solve this problem are by reducing particle size [4, 5] that leads to a shorter Li-ion diffusion path and higher electrode/electrolyte contact surface area [6]; or by doping with noble metals or oxides [7-9] into the LTO particles to improve high-rate discharge capacity and cycling stability through an increase in electrical conductivity and a

decrease in polarization of cathode [10, 11]; or by surface coating with a conductive phase to enhance surface electrical conductivity [12-17].

In fact, carbon coating of LTO particles has been proven to be the most effective and low cost way, since it improves the surface electrical conductivity and the electrical contact with electrolyte solution, which in turn leads to a significantly improved electrochemical performance with good rate capabilities [19-20]. Nevertheless, the question of how much carbon content and thickness (i.e., interfacial structure) to achieve the optimized coating effect still needs to be clarified. It has been reported that optimized carbon coating was to provide good conductivity and fast Li-ion diffusion [21, 22], however the presence of too much carbon has been proven unfavorable for attaining high capacities because of the Li^+ transport limited by barriers from the thick carbon layer [23–25]. The optimized thickness of the carbon layer has a major influence on ionic transport while slightly affecting the electrical conductivity [21, 22]. In a word, highly carbon coating could significantly improve the electrical conductivity but hinder the ion transport. Typically, the rate capability of the carbon-coated electrode material relies on both the ionic transport and electronic conductivity, which are greatly determined by the structure (graphitic or amorphous) and thickness of carbon layers [21-22]. Therefore, it is of great importance to optimize the carbon coating condition in order to improve the rate capability of electrode materials. Furthermore, it has been demonstrated that the optimal carbon coating with around 5 nm is the best to improve electrical conductivity and increase Li-ion diffusion simultaneously; and the enhanced electrode properties can be achieved by optimizing the content of the coated carbon in order to balance the electric conduction and the ionic transport [23-25].

Therefore, it is necessary to understand in depth the influence of the carbon coating on the electrode performance of the C-LTO composite. In this study, we prepared C-LTO anode particle materials with controlled carbon coating, and our structural characterization and electrochemical test revealed that the optimal amorphous carbon coating gives rise to increased effective electrical conductivity, resulting in enhanced electrochemical performance.

Experimental

Sample preparation

Firstly, micron-sized mixed C-$Li_4Ti_5O_{12}$ particles were hydrothermally synthesized using commercial anatase TiO_2 powders and some amounts of glucose as raw materials. In a typical synthesis, a stoichiometric amount (e.g., Ti:Li=5:4) of anatase TiO_2 powder (0.4 g) and glucose (0.7 g) was dispersed in $LiOH \cdot H_2O$ aqueous solution (60 ml). After stirring for 15 min, the suspension was transferred into a 50 mL Teflon-lined autoclave and heated at 180^{o}C for 15 hr. Subsequently, the white precipitate was filtered, and washed several times with deionized water to remove the excess hydroxide before drying at 80^{o}C for 6 hr. Finally, the micron-sized white powder was calcinated at 800^{o}C for 5 hr under Ar gas, followed by natural cooling in the furnace.

Structure characterization

Sample crystal structures were characterized by X-ray diffraction (XRD) on a INEL XRG 3000 diffractometer operating in transmission mode with Cu Kα radiation (λ = 0.15418 nm). Crystalline phases and carbon coating structure were characterized by high resolution TEM

imaging (HR-TEM) and selected area electron diffraction (SAED) using a JEOL 2010F FEG transmission electron microscope.

Scanning transmission X-ray microscopy (STXM) was conducted at the SM beamline of the Canadian Light Source (CLS). Powder sample of C-LTO was dispersed in methanol by brief sonication, and then deposited on Si_3N_4 windows for measurement. In STXM, the monochromatic X-ray beam is focused by a Fresnel zone plate to a ~30 nm spot on the sample, and the sample is raster-scanned with synchronized detection of transmitted X-rays to form images. Chemical/elemental mapping for a selected sample region of isolated particles was performed at the C, O K-edges, and Ti L-edge via two-energy image subtraction to generate optical density (od) image of each element distribution, e.g. 280/292 eV at C 1s. Image sequences (stacks) over a range of photon energies at these elemental edges were also acquired in order to obtain the X-ray absorption near edge structure (XANES) spectroscopy. Averaged XANES spectra were extracted from the combined image stack at the regions of submicron sized nanoparticles using an image mask which allows only selecting the region(s) of interest. STXM data were analyzed by aXis2000 (http://unicorn.mcmaster.ca/aXis2000.html).

Electrochemical test

Electrochemical measurements were performed using 2016-type coin cells assembled in an argon-filled glove box (German, M. Braun Co). To fabricate the electrodes, a mixture of the synthesized C-LTO particles, acetylene black, and polyvinylidene fluoride (PVDF) binder at a weight ratio of 80:10:10 was pasted on pure copper foil, and the electrode was dried at 80^{o}C for 12 hr in a vacuum oven. Pure lithium foil was used as the counter electrode. The electrolyte consisted of a solution of 1 M $LiPF_6$ in ethylene carbonate (EC) and dimethyl carbonate (DMC) with a volume ratio of 1 : 1 (EC+DMC). The cyclic voltammetry and rate cycle measurements were carried out between 1.0 and 2.5 V (vs. Li/Li^+) on a LAND-CT2001A battery-testing system.

Results and discussions

Structure Characterization

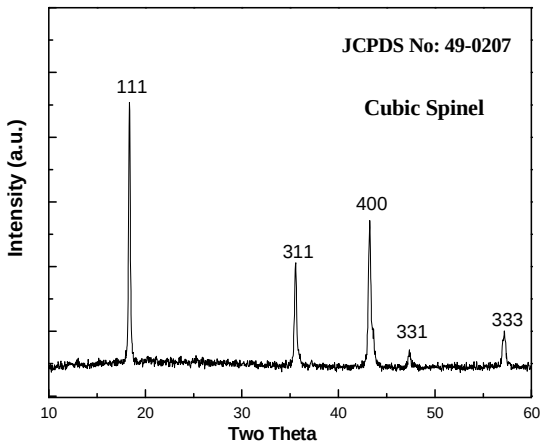

Figure 1. XRD pattern of C-LTO particles

Figure 1 is the XRD pattern of C-LTO particles. According to JCPDS data No: 49-0207, all the peaks in the XRD pattern can be indexed as the spinel cubic phase in the F*d3m* space group. Typically, no impurity peaks were found, indicating that the carbon coating did not influence the formation of cubic spinel LTO during preparation. Furthermore, it should be noted that no peaks belonging to carbon was detected, which is ascribed to the low content and/or the amorphous nature of carbon.

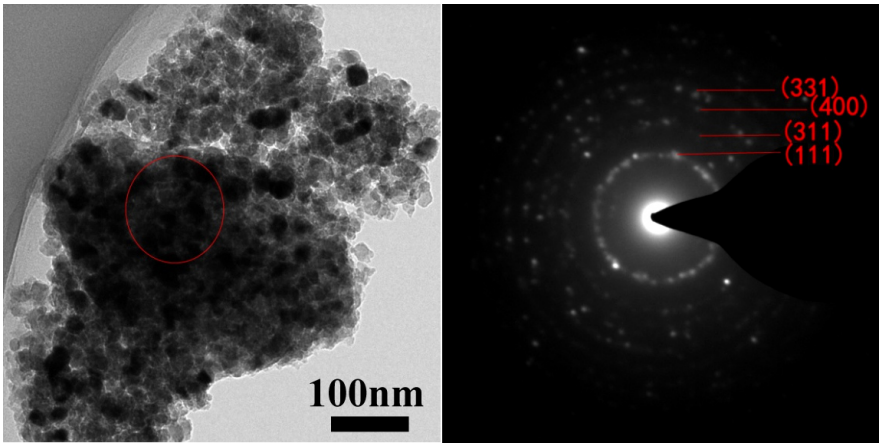

Figure 2. Typical TEM image (left) and SAED pattern (right) of C-LTO particles

Figure 2 shows the typical TEM image and SAED pattern of C-LTO particles. It is evident from the TEM image that LTO particles exhibit the spherical shape, and it is estimated that the average size is between 20-70 nm. The SAED pattern of Figure 2 was identified as the formation of spinel cubic crystal phase of LTO.

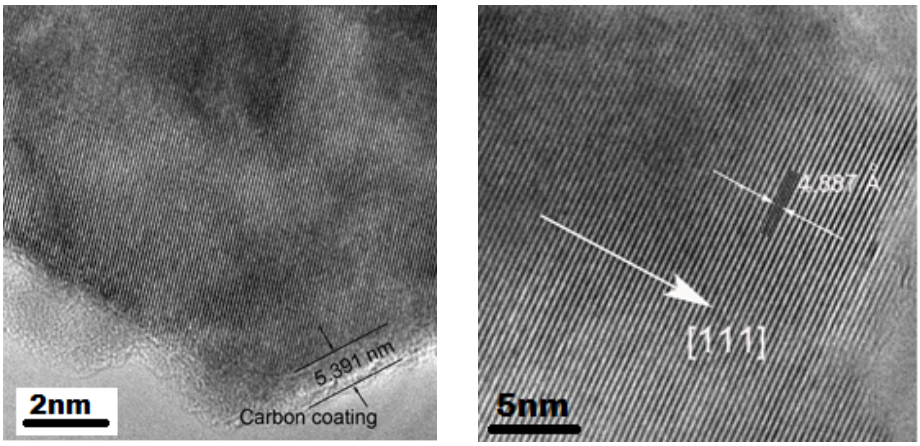

Figure 3. Typical HRTEM images of C-LTO particles

Nano-structures of individual C-LTO particles were further investigated by HR-TEM in Figure 3.

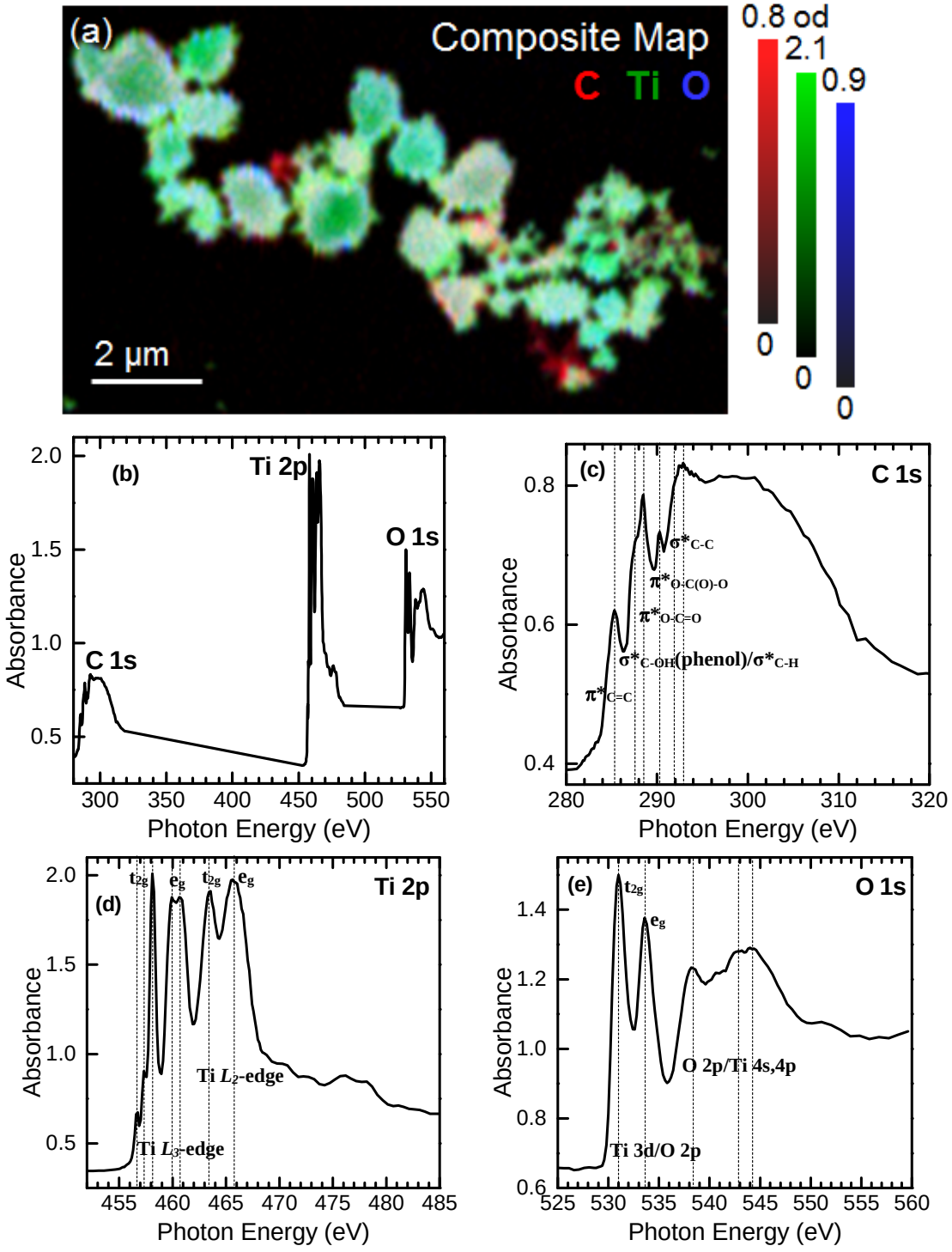

Figure 4. STXM chemical imaging and XANES spectra of C-LTO nanoparticles, (a) colour composite chemical map, red: carbon, green: titanium, blue: oxygen, all vertical color grey scales on the right represent sample optical density in each element; (b) all edges, (c) C 1s, (d) Ti 2p, and (e) O 1s XANES spectra of the selected submicron sized C-LTO nanoparticles. All vertical dashed lines in the spectra indicate the spectral regions of interest and are labelled with electronic structure assignments

It demonstrated the particles are well-crystallized and coated with around 5 nm amorphous carbon layers. It has been reported that the amorphous carbon nanolayers were formed during calcination process, and heating temperature and time during preparation are important factors to control the coating thickness [21-23]. Our sample calcination time is less than 5 hours in the protected environment, otherwise, carbon may disappear due to prolonged calcination time and potential reaction with oxygen. Meanwhile, the carbon layer acted as the dimension restrictor during high temperature calcination. HRTEM images further reveal that the clear lattice fringes have an inter-planar spacing of 0.48 nm, consistent with the spacing of the (111) atomic planes of the spinel structure, indicating that the well-crystallized spinel LTO phase was prepared.

STXM combined with XANES spectroscopy is a powerful synchrotron-based technique and widely used in studying the electronic and chemical structures of electrode materials for lithium ion batteries [26, 27]. Basically, each XANES spectrum is element-specific involving the excitation of electrons from a core level to local and partial empty states of a defined absorption atom, and offers the local bonding environmental information [28]. Chemical imaging can be performed based on XANES spectroscopy absorption contrast. Figure 4(a) displays STXM chemical/elemental imaging of some submicron sized C-LTO particles assemblies. It is evident that Ti and O are significantly abundant elements in the sample, while carbon intensity is much lower, yet still somehow uniformly distributed on the particle surface. This is consistent with the HR-TEM characterization revealing thin amorphous carbon coating on the LTO particles. Furthermore, quantitative XANES spectroscopy was obtained on the selected submicron sized C-LTO particles in the same sample region via STXM image stacks as a function of photon energy. Figure 4(b) shows the whole XANES spectrum extracted from the STXM stacks, which covers the C, O K-edges, and Ti L-edge. The relatively weak C 1s spectrum again reflects lower carbon content. More electronic structural details can be revealed from the XANES features at each elemental edge, as shown from Figure 4(c) to 4(e). C K-edge XANES (Figure 4(c)) indicates primarily amorphous sp^2 structure with C=C bonding (i.e. 285.3 eV) presented in the carbon content of the C-LTO particles, and strong oxygen functional groups present in the particles, presumably due to the bonding/interaction between the carbon coating and the nanoparticles through oxygen bonding bridges. Ti L-edge XANES (Figure 4(d)) suggested Ti^{4+} valence state and a significant crystal field splitting pertaining to the octahedral geometry for the core Ti^{4+} ion coordinated with six O^{2-} ions. Finally O K-edge XANES (Figure 4(e)) is found to be consistent with the octahedral Ti-O bonding and geometry in $Li_4Ti_5O_{12}$ spinel structure. To this end, both STXM and XANES results are in a good agreement with XRD, HR-TEM and SAED analysis.

Electrochemical Characterization

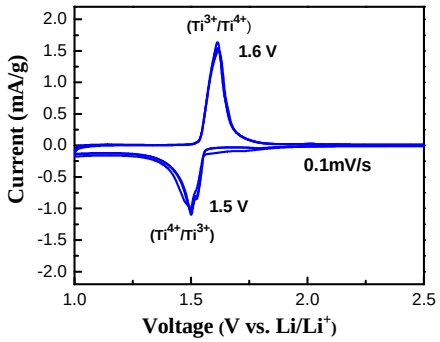

Figure 5. The CV curves for C-LTO particles

Figure 5 shows the cyclic voltammograms (CV) of C-LTO at scanning rates of 0.1 mV/s. A reversible pair of redox peaks is clearly observed within each curve, indicating only one well-defined step in the electrochemical process of reduction–oxidation for $Li_4Ti_5O_{12}$, corresponding to a cathodic and anodic process. The cathodic peak located around 1.50 V corresponds to the voltage plateau of the discharge process in which Li intercalates into the spinel $Li_4Ti_5O_{12}$. Meanwhile, the anodic peak located at 1.60V corresponds to the voltage plateau of the charge process in which Li de-intercalates from the spinel $Li_7Ti_5O_{12}$. This is a typical character of the $Li_4Ti_5O_{12}/Li_7Ti_5O_{12}$ two-phase reaction [29-32].

In addition, it is apparent that the initial three cycles almost overlap in the voltage between 1.0 and 2.5 V at a scan rate of 0.1 mV/s, demonstrating lithium insertion into and extraction from this electrode is reversible and the samples are pure and free of impurity phases.

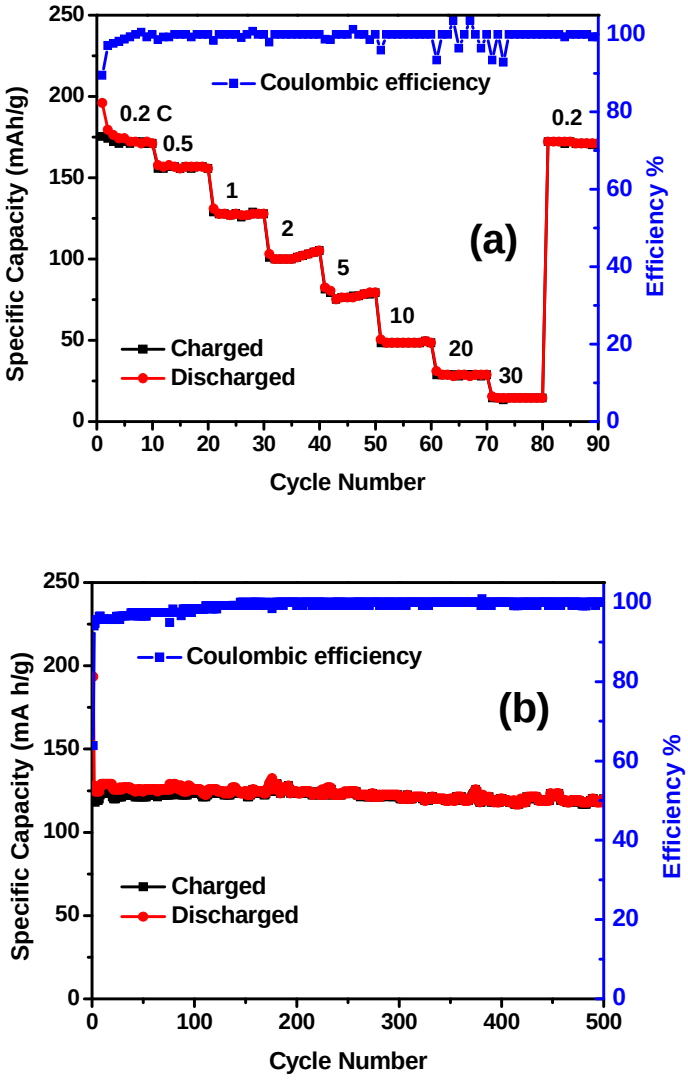

Figure 6. Rate (a) and cycling performance (b) of C-LTO particles

Figure 6 (a) shows the rate cycle performance and discharge capacity retention of the C-LTO particles electrode during cycling at various C-rates over the voltage cut-off range of 1.0–2.5 V. The electrode was progressively charged and discharged in a series of stages with rates from 0.2C to 30C. For each stage, the charge–discharge process was taken for 10 cycles.

It can be seen from the Figure 6(a) that the discharge capacity of the LTO electrode decreases with increasing C-rate, mainly due to polarization. Also, it was measured that in the charge–discharge stages with rate 0.2C–30C, the discharge capacity remained stable. It shows that the initial discharge capacity of the sample at 1C is 125 mAh/g; and compared to the initial discharge capacity at 0.2C, the capacity retains 84%. As shown in Figure 6(b), an excellent cycling performance is observed, even at the high rate of 1C. The capacity loss is only in the range of 0.04% within each 100 cycles, indicating the high stability in repeated cycles. In addition, the coulombic efficiency stayed at about 100%, demonstrating an excellent cycling performance of the C-LTO particles electrode.

Apparently, this enhancement could be associated with the smaller particle size and the presence of electrically conductive carbon coating. It was reported that too low carbon content could barely improve the electrical conductivity while too much carbon would hinder the ionic conductivity [23-25]. Generally, the charge-transfer reaction takes place at the LTO electrode when accepting both Li^+ and electrons. For bare LTO, the particle surface is easily accessible by Li^+, but suffers from the lack of electrical conductivity. Electron conduction is facilitated by the carbon coating. For Li^+ transport, there is a facile way to reach the LTO particle surface that is coated by a thin carbon layer. In the presence of a thick carbon layer, the Li^+ diffusion path may be blocked due to graphitic stacking. This hampers ionic diffusion and accounts for the limited rate capability of the C-LTO particle. Thus a critical balance between the electronic and the ionic transport is necessary to attain remarkable performance by optimizing the carbon coating content and thickness [33, 34].

It can be concluded that, the high-rate charge–discharge capability of our as-prepared C-LTO electrode could only be deduced from increased electrical conductivity and facile Li^+ ion diffusion in the optimized nano-carbon coating structures [35, 36].

Conclusions

Carbon-coated LTO anode materials for the lithium ion battery are successfully prepared. Comprehensive structural characterizations and chemical analyses (HRTEM imaging, SAED patterns, STXM imaging, and XANES spectra) revealed that the as-prepared C-LTO particles have a well-developed spinel nanocrystal structure with average size between 20-70 nm, and exhibited the spherical shape with around 5 nm uniform amorphous carbon layer coated on their surface. It has been demonstrated that the optimized amorphous coating layer is beneficial to improve the kinetic process and is favorable for fast electron transport. It improves electrical conductivity and effectively reduces the polarization of the LTO electrode. As a result, the C-LTO electrode presents an excellent performance in terms of rate capability, cycling life, capacity retention, and coulombic efficiency. This excellent electrochemical performance makes the C-LTO anode a promising material for high-rate rechargeable energy storage lithium-ion batteries.

Acknowledgments

The financial supports from the President's Award of University of Waterloo and Postgraduate Scholarships from the Natural Sciences and Engineering Research Council of Canada (NSERC) and Nano-fellowship from Waterloo Institute for Nanotechnology (WIN) are greatly appreciated by XC Sun.

References

1. T. Ohzuku, A. Ueda, and N. Yamamoto, J. Electrochem. Soc., **142,** 1431 (1995).
2. P. G. Bruce, B. Scrosati, and J.M. Tarascon, Angew. Chem., Int. Ed., **47,** 2930 (2008).
3. T. F. Yi, L. J. Jiang, J. Shu, C. B. Yue, R. S. Zhu, and H. B. Qiao, J. Phys. Chem. Solids, **71**, 1236 (2010).
4. K. Zaghib, M. Simoneau, M. Armand, and M. Gauthier, J. Power Sources, **81-82**, 300 (1999).
5. C. H. Chen, J.T. Vaughey, A.N. Jansen, D. W. Dees, A.J. Kahaian, T. Goacher, and M. M. Thackeray, J. Electrochem. Soc., **148,** A102 (2001).
6. L. Cheng, H, J. Liu, J. J. Zhang, H. M. Xiong, and Y. Y. Xia, J. Electrochem. Soc., **153**, A1472 (2006).
7. C. Jiang, E. Hosono, M. Ichihara, I. Honma, and H. Zhou, J. Electrochem. Soc., **155**, A553 (2008).
8. S.Y. Yin, L. Song, X.Y. Wang, M. F. Zhang, and Y.X. Zhang, Electrochim. Acta, **54,** 5629 (2009)
9. S. Jia, J. Zhang, W. Wang, Y. Huang, Z. Feng, Z. Zhang, and Z. Tang, Mater. Chem. Phys., **123**, 510 (2010).
10. S. H. Huang, Z.Y. Wen, X.J. Zhu, and X. L. Yang, J. Elctrochem. Soc., **152**, A1301 (2005).
11. S. H. Huang, Z.Y. Wen, X. L. Yang, Z. H. Gu, and X. H. Xu, J. Power Sources, **148**, 72 (2005).
12. A. Sivashanmugam, S. Gopukumar, R. Thirunakaran, C. Nithya, and S. Prema, Mater. Res. Bull., **46,** 492,(2011).
13. T. Yuan, R. Cai, and Z.P. Shao, J. Phys. Chem. C, **115,** 4943 (2011).
14. Y. Shi, L. Wen, F. Li, and H.M. Cheng, J. Power Sources, **196,** 8610 (2011).
15. L. Cheng, X.L. Li, H.J. Liu, H.M. Xiong, P.W. Zhang, and Y.Y. Xia, J. Electrochem. Soc., **154,** A692 (2007).
16. H.G. Jung, J. Kim, B. Scrosati, and Y.-K. Sun, J. Power Sources, **196**, 7763 (2011).
17. L. Yang, and L. Gao, J. Alloys Compd., **485, 93** (2009).
18. L. Zhao, Y.S. Hu, H. Li, and Z. Wang, and L. Chen, Adv. Mater., **23, 1385** (2011).
19. M. Inagaki, Carbon, **50, 3247** (2012).
20. H. Q, Li and H.S. Zhou, Chem. Commun., **48**, 1201 (2012).
21. G.N. Zhu, C. X. Wang, and Y.Y. Xia, J. Electrochem. Soc, **158**, A102 (2011).
22. Z.Q. Zhu, F.Y. Cheng and J. Chen, J. Mater. Chem. A, **1**, 9484 (2013)
23. J. Wang, X. M. Liu, H. Yang and X. D. Shen, J. Alloys Compd., **509**, 712 (2011)
24. M. Gaberscek and J. Jamnik, Solid State Ionics, **177**, 2647 (2006).
25. R. Dominko, M. Bele, M. Gaberscek, M. Remskar, D. Hanzel, S. Pejovnik and J. Jamnik, J. Electrochem. Soc., **152**, A607 (2005).

26. J. Wang, J.G. Zhou, Y. F. Hu and T. Regier, Energy Environ. Sci., **6**, 926 (2013)
27. H. B. Zhang, J. Wang, X.L. Pan, Y.F. Hu, and X. H. Bao, J. Chem. Phys., **136**, 174701 (2012).
28. S. Yang, D.N. Wang, G.X. Liang, Y.M. Yiu, J.J. Wang, L.J. Liu, X.L. Sun and T.K. Sham, Energy Environ. Sci., **5**, 7007 (2012).
29. T. Ohzuku, A. Ueda, and N. Yamamoto, J. Electrochem. Soc., **142**, 1431(1995).
30. S. Huang, M. Woodson, and R. Smalley, J. Liu, Nano Lett., **4**, 1025 (2004).
31. H. G. Jung, M. W. Jiang, J. Hassoun, and Y. K. Sun, B. Scrosati, Nat. Commun. **2**, 516 (2011).
32. Z. Liang, Y. S. Hu, H. Li, Z. X. Wang, L. Q. Chen, Adv. Mater., **23**, 1385 (2011).
33. J. X. Tang and L. J. Gao, Phys. Scr., **85**, 045802 (2012).
34. B. H. Li, F. Ning, Y. B. He, H. D. Du, Q. H. Yang, J. Ma, F. Y. Kang, and C. T. Hsu, Int. J. Electrochem. Sci., **6**, 3210 (2011).
35. J. Z. Chen, L. Yang, S. H. Fang and Y. F. Tang, Electrochimica. Acta, **55**, 6596 (2010).
36. Z. S. Hong, X. Z. Zheng, X. K. Ding, L. L. Jiang, M. D. Wei and K. M. Wei, Energy Environ. Sci., **4**, 1886 (2011).